nature chemistry

ARTICLES

PUBLISHED ONLINE: 19 MARCH 2009 | DOI: 10.1038/NCHEM.130

Catalytic behaviour of dense hot water

Christine J. Wu*, Laurence E. Fried, Lin H. Yang, Nir Goldman and Sorin Bastea

Water is known to exhibit fascinating physical properties at high pressure and temperature. Its remarkable structural and phase complexities suggest the possibility of exotic chemical reactivity under extreme conditions, although this remains largely unstudied. Detonations of high explosives containing oxygen and hydrogen produce water at thousands of kelvin and tens of gigapascals, similar to conditions in the interiors of giant planets. These systems thus provide a unique means of elucidating the chemistry of 'extreme water'. Here, we show that water has an unexpected role in catalysing complex explosive reactions—contrary to the current view that it is simply a stable detonation product. Using first-principles atomistic simulations of the detonation of the high explosive pentaerythritol tetranitrate, we discovered that H_2O (source), H (reducer) and OH (oxidizer) act as a dynamic team that transports oxygen between reaction centres. Our finding suggests that water may catalyse reactions in other explosives and in planetary interiors.

Water, one of the most abundant materials on the Earth's surface and in the interiors of Uranus and Neptune[1], is famous for its complexity and abnormal behaviour[2–9]. Under ambient conditions, many of the abnormal properties of water, such as its unusually large heat capacity, melting temperature and dielectric constant, are known to be the result of pronounced hydrogen bonding between water molecules. At pressures above 26 GPa, other exotic behaviour is found as hydrogen bonding is lost[8] and covalent interactions are substantially weakened. For instance, on the basis of quantum simulations, it has been predicted that water becomes a superionic solid above 22 GPa and 1,500 K, dissociates into an ionic liquid above 3,500 K and transforms into a metallic phase above 7,000 K (ref. 2). Diamond anvil cell experiments[5] and quantum molecular dynamics (MD) simulations[6] have confirmed the presence of a superionic solid at elevated conditions (about 47 GPa, 1,500 K). This phase is characterized by fast hydrogen-ion diffusion through a body-centred-cubic oxygen network. Given the dramatic alterations in the structure and bonding characteristics of water that occur under extreme conditions, it is possible that these exotic water phases exhibit unique chemical behaviour.

To probe the chemical properties of extreme water, one needs to go beyond pure water. Water more commonly acts as a solvent or a reactant (for example supercritical water[10]). In addition, water has been found to act as a 'physical' catalyst[11–13] in some reactions, in which the catalytic ability of water is associated with its physical interactions with reactants. For instance, water increases rates of solvolytic reactions owing to its enhancement of charge screening as an effective dielectric medium[11]. It has been reported that water accelerates the reaction between hydroxyl radicals and acetaldehyde because of its ability to form hydrogen bonds with acetaldehyde, analogous to a substrate in heterogeneous catalysis[12,13].

Here, we report novel 'chemical' catalytic behaviour of water, promoting oxygen transport in the Chapman–Jouguet (CJ) state. The CJ state is the sonic point behind a shock front at which the energy of the detonation wave has been completely released[14,15]. The thermodynamic condition of the CJ state achieved at chemical equilibrium determines the propagation rate and pressure of a detonation wave[14,15]. Using density functional theory (DFT) MD simulations for a time of 11 ps, we discovered that the team of H_2O, H and OH transports oxygen from nitrogen storage to carbon fuel during pentaerythritol tetranitrate (PETN) decomposition reactions at the estimated CJ detonation condition[15] ($\rho = 2.38$ g cm^{-3}, $T = 4{,}200$ K), and also at somewhat lower temperature ($\rho = 2.38$ g cm^{-3}, $T = 3{,}000$ K). Under both temperature conditions, 'extreme water' serves both as an end product and as a key chemical catalyst.

The observed catalytic behaviour of water in PETN reactions challenges the traditional view of water in high-explosive chemistry[16–24]. For a molecular high explosive that consists of carbon, nitrogen, oxygen and hydrogen (for example PETN), the three major gaseous products are known to be water, carbon dioxide and molecular nitrogen[14,15]. However, the chemical processes leading to these stable compounds are not well understood[16–24]. At present, these products are assumed to form a molecular mixture at the CJ state[14]. In contrast, we find that water forms much more rapidly than carbon dioxide and molecular nitrogen during PETN thermal decomposition. Subsequently, water substantially accelerates the formation of carbon dioxide and molecular nitrogen. Further, we find that, under the CJ condition, the lifetime of a molecule is so short that it is comparable to that of a molecular vibration, which calls the very concept of a molecule into question[25]. As a result, the traditional approach based on molecular reactions that is commonly applied in gas-phase combustion chemistry is no longer adequate for describing chemical reactions under these extreme conditions. In this context, we suggest that the progress of condensed-phase explosive reactions may be treated as an oxygen-transport problem.

Results and discussion

Details of the simulation method and analysis are provided in the Methods section. Figure 1a shows the unreacted PETN molecular crystal structure before decomposition. Chemical reactions started when the system was heated to the desired temperature. MD snapshots were saved every 6 fs for post-simulation analysis. To analyse reactions, we have developed a molecular analyser code that determines the chemical species, lifetimes, reaction events and rates on the basis of simulation trajectories.

To demonstrate visually how chemical reactions are traced from simulation trajectories, in Fig. 1b,c we display two MD snapshots that show the hydrogen, oxygen and nitrogen atoms before and after a reaction. The reaction shown creates molecular nitrogen in a background of dense atomic fluid, a key step of energy release. Owing to the dense and highly reactive environment, it is difficult

Lawrence Livermore National Laboratory, 7000 East Avenue, Livermore, California 94551, USA. *e-mail: wu5@llnl.gov

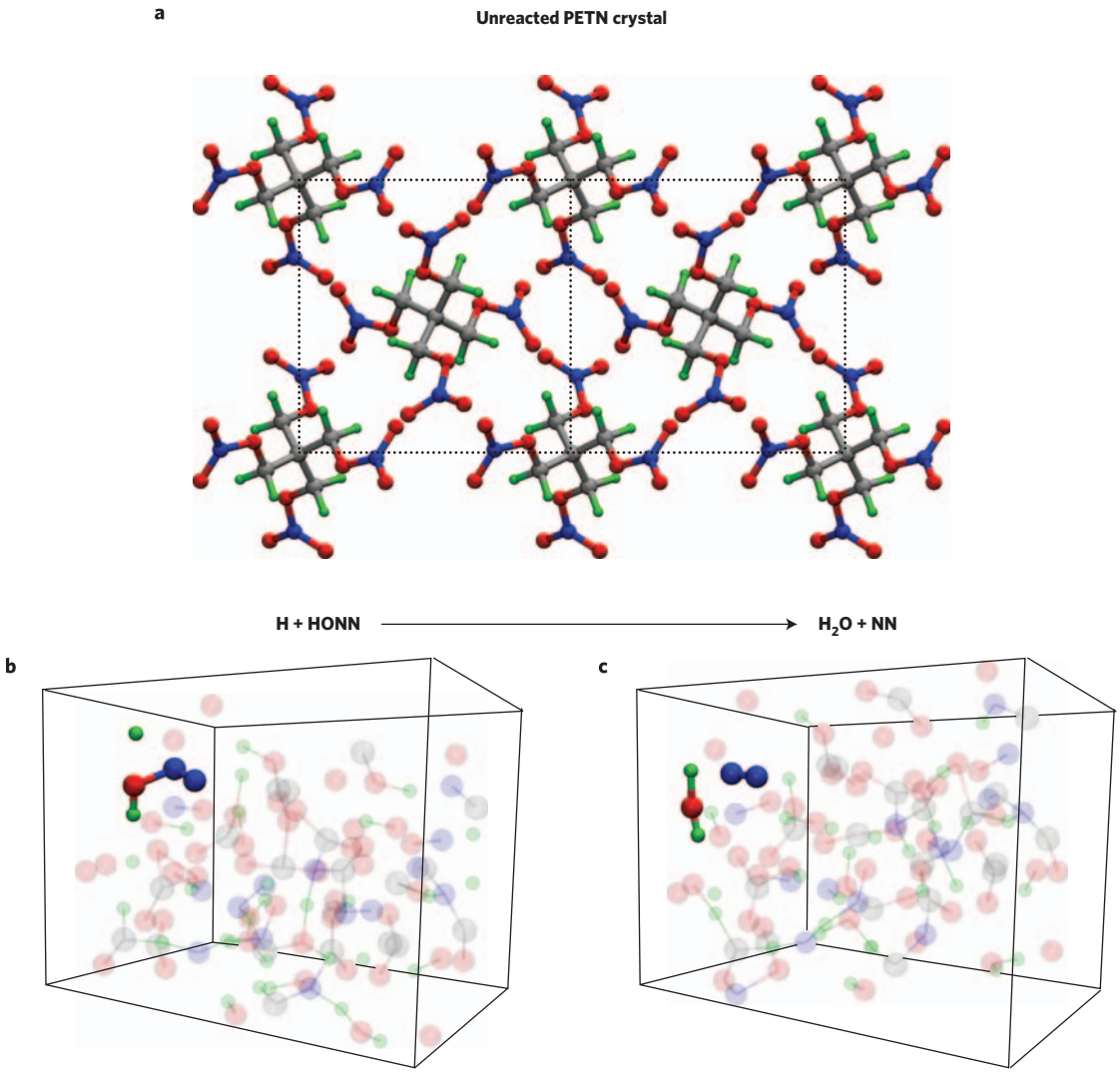

Figure 1 | Initial MD configuration and example simulation snapshots. a, Unreacted PETN crystal viewed from the [001] direction. **b**,**c**, Two configurations at 4,200 K showing the left and right sides of the reaction $H + HONN \rightarrow H_2O + N_2$. This demonstrates that H and OH have major roles in catalysing N_2 formation. For clarity, other atoms in the simulation cell are rendered with transparency. Nitrogen, oxygen, carbon and hydrogen are coloured blue, red, grey and green, respectively.

to determine key chemical kinetics on the basis of the connectivity of bonding alone. For instance, at 4,200 K, we have determined over 3,000 unique reactions, 78% of which only occur once in the simulation. By painstakingly tracing key reactions among snapshots, we found that many reactions occur locally. Specifically, the same type of functional group transformation (that is, a local reaction) may occur for reactions involving different molecules.

In a PETN crystal, oxygen is stored as NO_2 groups. The progression of the PETN reaction can be viewed as the flow of oxygen from storage sites (NO or NO_2) to fuel sites such as carbon (forming CO or CO_2) or hydrogen (forming H_2O). When we analysed the key local reactions that lead to the formation of carbon dioxide and molecular nitrogen, we observed an intriguing catalytic function of H_2O, OH and H. The catalysis can be visualized by considering local reaction centres. First, we found that nitrogen loses its oxygen mostly to hydrogen, not to carbon, even after the concentration of water reaches equilibrium. Second, we observed that carbon atoms capture oxygen mostly from OH, rather than directly from NO or NO_2. The H_2O dissociates and recombines with H and OH frequently; thus, a steady concentration of H and OH is maintained.

A schematic of this catalytic cycle is outlined in the reaction flowchart in Fig. 2a, which illustrates how H and OH catalytically transport oxygen from NO_2 to CO, thus forming CO_2. First, dissociating H_2O provides both oxidizing OH species and reducing H atoms. In the reduction cycle, H and ONO form an intermediate species, HONO. Then, HONO dissociates into OH and NO. In essence, hydrogen acts as a reducer and removes oxygen from NO_2 groups. In contrast, OH acts as an oxygen donor to carbon compounds that are not fully oxidized. For instance, in the oxidation cycle, OH reacts with CO to form HOCO, which then becomes H and CO_2. The net result of this oxidation process is the transport of oxygen (shown in red) from OH to CO, thus producing CO_2. Recombination of OH and H produces H_2O again. In comparison, the process $OH + CO \rightarrow H + CO_2$ also has an important role in hydrocarbon combustion, where OH is a key free radical and H_2O_2 is the source[26,27]. During PETN reactions, H_2O (with OH) acts as an oxidizer only when it reacts with carbon. When H_2O (with H) reacts with NO_2 groups, it acts as a reducer.

Catalysts are reagents that accelerate chemical reactions without being consumed. The above example shows that H_2O, with H and OH, participates in the overall reaction $CO + NO_2 \rightarrow CO_2 + NO$

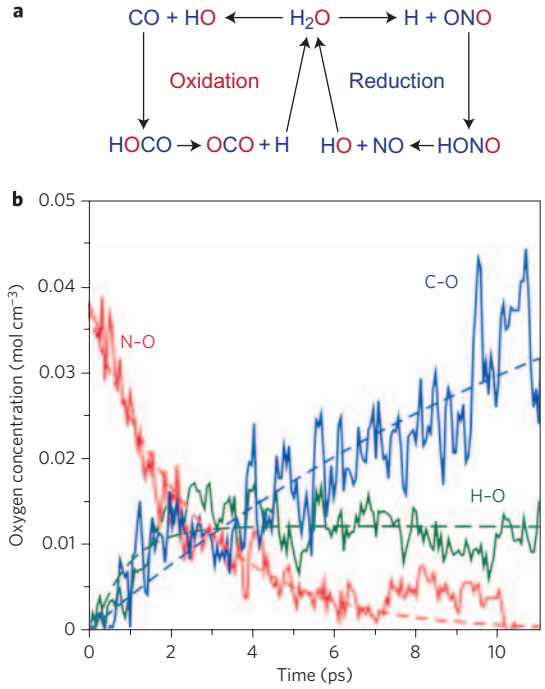

Figure 2 | Catalytic cycle of local reaction centres, demonstrating oxygen transportation from nitrogen to carbon and hydrogen. a, Schematic drawing of a typical set of reactions where oxygen (red) flows from nitrogen to carbon. **b**, Time dependence of the concentrations of oxygen bonded with hydrogen (for example OH and H_2O, green), nitrogen (for example NO_3, NO_2 and NO, red) and carbon (for example CO and CO_2, blue) at 3,000 K. Formations of C–O and N–O bonds increase and decrease with time, respectively, whereas the H–O bond number remains roughly constant after initial formation. This suggests catalysis mediated by OH. The dashed lines are analytical fits of solid lines to reflect the overall trend.

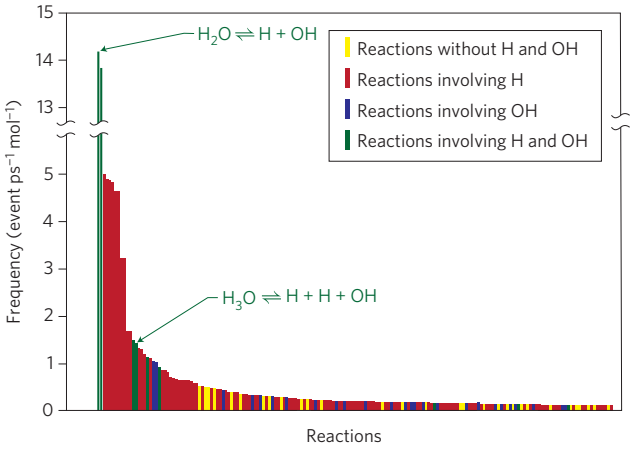

Figure 3 | Overwhelming participation of hydrogen in the majority of reactions. Frequencies (event ps^{-1} per PETN molecule) of the 176 most frequent reactions obtained at $T = 4{,}200$ K.

without being consumed. We have produced a time history of the bonding of oxygen during the overall reaction, which sheds additional light on how this catalysis accelerates oxygen transport. In Fig. 2b, the number of oxygen atoms bonded with nitrogen decreases with time (red curve) whereas the number of oxygen atoms captured by carbon as species of CO and CO_2 increases (blue curve) as the reaction progresses. Note that, after the initial production of water, the oxygen content associated with H (such as OH and H_2O) oscillates around a relatively constant average (green curve), at the same time that oxygen atoms are transported from nitrogen to carbon. The individual concentrations of H and OH also achieve nearly constant values during this time period (not shown), indicating typical catalytic behaviour.

The overwhelming participation of H and OH in the chemical reactions of PETN is further illustrated in Fig. 3, in which each column represents one unique elementary reaction identified by our molecular analyser on the basis of the entire MD trajectory. For instance, the first column represents the reaction of $H + OH \rightarrow H_2O$. Only the 176 most frequent reaction types are shown on the plot. Correspondingly, the slowest reaction shown on this plot has a rate of roughly once every 10 ps per PETN. Among the top 176 reactions, 118 involve H, 25 involve OH, and 9 involve both H and OH. Only 24 reactions did not involve H or OH. Among all 3,000 unique reaction events identified from the simulation at 4,200 K, more than 76% involve H atoms.

Three factors are crucial contributors for this catalytic cycle: (1) formation of water before production of carbon dioxide and molecular nitrogen, making it an available catalyst; (2) fast dissociation of H_2O to generate the oxidizer OH and the reducer H; and (3) accelerated hydrogen mobility that enables fast transport of oxygen between species. The first factor is largely due to the unique molecular structure and composition of PETN. In comparison, the second and third factors are associated with extreme conditions.

The formation of water is extremely fast: water appears after only 18 fs at 4,200 K, and it is produced much more rapidly than carbon dioxide or molecular nitrogen. The time sequence can be explained largely by the relative proximity of hydrogen to oxygen in comparison with other atoms in a PETN molecule (shown in Fig. 1a). The closer the reactants, the shorter time it takes to form products. On heating, PETN dissociates, producing mobile H and NO_2 groups. The short distance between the H atoms and the NO_2 in PETN provides an environment for the fast reaction of $2H + NO_2 \rightarrow HONO + H \rightarrow H_2O + NO$. Further reduction of NO to molecular nitrogen is a much slower process because nitrogen atoms are far from each other in the unreacted PETN molecule and atomic nitrogen is much less mobile and has a lower concentration than atomic hydrogen. In fact, at 4,200 K, the first nitrogen molecule is formed from an intermediate species, NNO, after 1 ps. Reduction of NNO to molecular nitrogen is also carried out by two hydrogen atoms: first to HONN (Fig. 1b) and then to H_2O and N_2 (Fig. 1c) via $H + HONN$. Note that the key process leading to formation of molecular nitrogen is the transport of oxygen from NO_2 groups to hydrogen.

Under extreme conditions, the dissociation of water occurs at a much higher rate and by a different mechanism than under ambient conditions. On average, water molecules do not live very long. As Fig. 3 shows, $H_2O \rightarrow H + OH$ is the most frequent event, at about 14 events ps^{-1} per PETN molecule, and its reverse reaction ranks second. In contrast, under ambient conditions, water dissociates predominantly by the bimolecular reaction $2H_2O \rightarrow H_3O^+ + OH^-$ (ref. 28). At the CJ condition, the bimolecular water dissociation pathway occurs at a much lower frequency (about 1.6 events ps^{-1} per PETN). Our observation of the unimolecular dissociation mechanism is consistent with previous experiments. For instance, Holmes *et al.*[8] reported that the Raman spectra of H_3O^+ associated with the intermolecular hydrogen bonds vanish at 26 GPa, which led them to support the unimolecular mechanism. In contrast, Schwegler *et al.*[9] reported that water dissociates via the bimolecular mechanism, on the basis of quantum simulations of pure water at 2,000 K. The discrepancy between our result and that of Schwegler *et al.*[9] is probably due to the difference in simulation temperatures (2,000 K in ref. 9 and 3,000–4,200 K in our work) and water concentration (pure versus

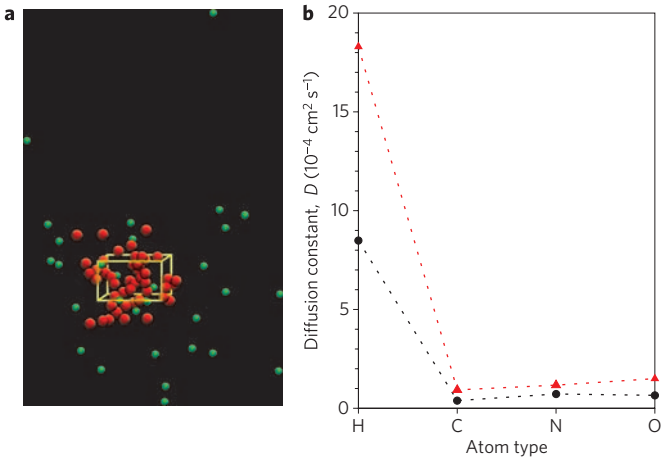

Figure 4 | Hydrogen is more mobile than other heavier atoms. a, Snapshot of hydrogen (green) and oxygen (red) positions at 8.95 ps, $T = 4{,}200$ K, with periodic boundary conditions removed to track their distances travelled. The simulation cell (yellow box) indicates the initial boundary of hydrogen and oxygen atomic positions at time = 0. **b**, Diffusion constants of hydrogen, carbon, nitrogen and oxygen atoms obtained at $T = 3{,}000$ K (black dotted line) and 4,200 K (red dotted line) at $\rho = 2.38$ g cm^{-3}.

mixture). The bimolecular dissociation mechanism is expected to be favoured at lower temperature and higher water concentration.

The rapid dissociation of water enables it to be a continuous source of oxidizing (OH) and reducing (H) agents, a property that is unique to 'extreme water'. It also implies that bonds containing hydrogen are inherently non-molecular, and thus the CJ state should not be treated as a mixture of conventional molecules, as has been assumed[14]. This observation is consistent with a recent quantum MD study of shocked nitromethane[25].

The mobility of hydrogen in these mixed fluids is far greater than that of the heavier elements. Figure 4a shows a snapshot of hydrogen atoms (green) and oxygen atoms (red) after 8.98 ps at 4,200 K. To show atomic mobility with distances travelled, the atomic positions are shown with the periodic boundary conditions removed. Obviously, hydrogen atoms have travelled much further than oxygen atoms from their initial positions inside the simulation cell. Similar behaviour of hydrogen was previously found for pure water[9]. Figure 4b illustrates the diffusion constants of hydrogen, carbon, nitrogen and oxygen atoms at 3,000 K (black dotted line) and 4,200 K (red dotted line). At 4,200 K, hydrogen atoms diffuse at a rapid rate of 1.83×10^{-3} cm^2 s^{-1}. As a comparison, hydrogen diffuses at a slower rate of 3×10^{-4} cm^2 s^{-1} in the superionic phase of water ($\rho = 2.6$ g cm^{-3}, $T = 2{,}000$ K)[6].

To better understand the mechanism of hydrogen transport, we performed a simulation in which the motions of elements other than hydrogen were frozen at the positions obtained from the 4,200 K simulation at 6 ps. We found that the hydrogen diffusion constant increased to 4.3×10^{-3} cm^2 s^{-1}, indicating that hydrogen transport can be thought of as random diffusion through a slowly evolving matrix of heavy atoms, an approximation applied to our conductivity calculation (shown later). Furthermore, we found that hydrogen mobility is thermally activated. As we decreased the temperature to 3,000 K, the hydrogen diffusion constant decreased to 8.5×10^{-4} cm^2 s^{-1}.

So far, we have not addressed the electronic characters of H, OH and major products. In particular, are the species best described as ions (for example in solution chemistry) or as radicals (for example in combustion)? Figure 5 shows charge histograms of carbon, nitrogen, hydrogen and oxygen atoms at the end of simulation at 4,200 K. Note that carbon and nitrogen charge distributions are approximately centred around neutrality (Fig. 5a,b), which is consistent with the charge neutrality found for CO, CO_2 and N_2. In comparison, hydrogen and oxygen have noticeable net charges (for example H ($+0.3e$), and OH ($-0.16e$)) on average. As a result, oxygen has a bimodal distribution depending on whether it bonds to hydrogen or to carbon. The overall fluid has a root-mean-square charge separation $\langle q^2 \rangle^{1/2} = 0.3e$, the same as the average charge on hydrogen. The average atomic charges correlate with the Pauling electronegativity[29]. Hydrogen, the element with the lowest electronegativity (2.1), has net positive charge, whereas oxygen, the element with the highest electronegativity (3.5) has net negative charge. Carbon and nitrogen, with intermediate electronegativity, have no net charge.

Estimating the background dielectric constant of a CJ fluid experienced by the mobile ions provides important information about dielectric screening, a key factor in determining the relative stability of a radical and an ion. We have estimated an upper bound on the dielectric constant of the CJ mixture with another method, in which the calculation used the concentrations of neutral species predicted by the thermal chemistry code Cheetah[15] at the CJ condition. In this case, a simple extension to mixtures of the method applied in a previous study[30] of supercritical water yields a dielectric constant $\varepsilon \approx 2$. This suggests that the behaviour of a hot, dense fluid at the CJ condition is more similar to a molten salt[31,32] or a polymer (for example polytetrafluoroethylene[33], $\varepsilon \approx 2$) than a standard ionic solution ($\varepsilon \approx 100$) or a gas-phase mixture ($\varepsilon \approx 1$).

A comparison with the experimental d.c. electrical conductivity[34] provides an important verification of our MD results on the charge characteristics of the CJ fluid. From analysing the time-dependent electronic structure of the simulations, we learned that the CJ fluid near chemical equilibrium is an electronic insulator, although temporary metallization was observed near the height of chemical reactivity (see Supplementary Information). Thus, an ionic conduction mechanism determines the electrical conductivity σ of the system. To calculate the ionic conductivity of the CJ fluid, we assumed that hydrogen atoms ($+0.3e$) move in a background of slowly evolving heavy atoms of average charge $-0.3e$. Using the Nerst–Einstein relation[35], averaged charges and diffusion constants of fast and slow populations, we estimated σ to be about 70 Ω^{-1} m^{-1} (see Methods). This value is in excellent agreement with the experimental value of 60 Ω^{-1} m^{-1} measured for PETN at the CJ condition[34].

Conclusions

This catalytic mechanism is completely different from previously proposed decomposition mechanisms for PETN[16–20] or for similar explosives[21–25], in which water is just an end product. It shares a certain similarity with hydrocarbon combustion, in that OH has an important role in converting CO to CO_2 (refs 26,27), although they are substantially different. For instance, H_2O is the source of OH instead of H_2O_2 (refs 26,27) in combustion. In addition, in a dense, hot fluid, OH and H are partially charged, not neutral, and their concentrations remain nearly unchanged after initial formation. In contrast, the radical population grows in combustion and vanishes after burning. Given the active role played by H_2O, H and OH in detonation chemistry, it is conceivable that the kinetics of water formation may also contribute to high-explosive sensitivity (the ease of initiating a violent reaction). Furthermore, the chemistry of 'extreme water' also has important implications for planetary science. The conditions of high-explosive detonation are similar to those in the interiors of giant planets such as Uranus and Neptune[1]. The interiors of these planets are expected to be composed primarily of hydrogen, carbon, nitrogen and oxygen, as is PETN. Our results show that hydrogen atoms retain the high mobility at extreme conditions that was found in previous work on pure H_2O (refs 2,6 and 9) and NH_3 (ref. 2), even when mixed with substantial quantities of carbon. The catalytic activity

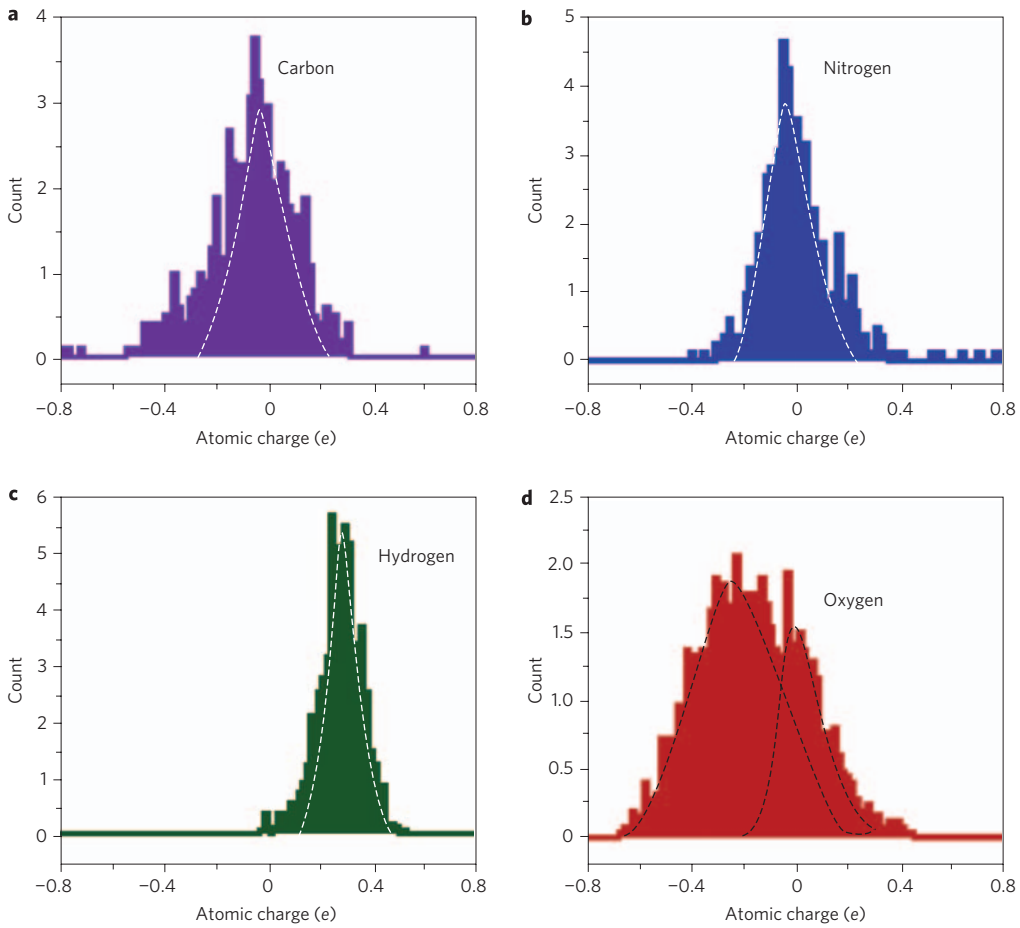

Figure 5 | Atomic charge distributions obtained at the Chapman–Jouguet condition. Charge histograms of atoms obtained from Mulliken population analysis on 30 consecutive configurations near the end of the 4,200 K simulation: **a**, carbon; **b,** nitrogen; **c,** hydrogen; **d,** oxygen.

of water found here suggests that the chemistry of these planetary interiors may be very fast, maintaining chemical equilibrium even in the presence of very unreactive species such as diamond.

Methods

DFT/MD simulations. Under ambient conditions, the most stable form of PETN is a molecular crystal of the $P\bar{4}2_1c$ space group[36,37] (shown in Fig. 1a), which consists of two molecules per unit cell. We started with an uncompressed cell containing 4 PETN molecules per 116 atoms based on a $1 \times 1 \times 2$ supercell and an experimental geometry of 9.38 Å × 9.38 Å × 13.418 Å. We then uniformly scaled the crystal axes in several steps until the estimated CJ density of 2.38 g cm^{-3} was achieved. At each step, we minimized the energy of the configuration.

We used a code developed by one of the authors (L.H.Y.) to perform DFT/MD simulations for constant particle number, volume and temperature (NVT) ensembles[38]. The code uses a pseudopotential treatment of core electrons and a plane-wave basis set[38]. Dynamics are based on the Born–Oppenheimer approximation. The code is specifically designed to take advantage of the massively parallel architecture of the teraflop computer Blue Gene/L at Lawrence Livermore National Laboratory. Three-dimensional periodic boundary conditions were applied to mimic a solid environment. The NVT condition is comparable to those produced by heated diamond anvil cells or thermal ignition experiments, which are different from detonations, in which a wider range of densities and temperatures are experienced. We believe that the chemical kinetics at a well-defined NVT condition are likely to shed light on other extreme conditions, such as shock (for further discussion of the similarity between reactions under shock and at constant volume, see Supplementary Information).

We used the Perdew–Burke–Ernzerhof[39] (PBE) exchange-correlation function and a single k-point. Core electrons were represented by Troullier–Martins pseudopotentials[40], with a kinetic-energy cutoff of 80 Ry (ref. 6). The electron temperature was set to be the same as the ion temperature using Fermi–Dirac smearing. A time step of 1.2 fs was used in time integration. The NVT simulations[41] were performed at 4,200 and 3,000 K. Snapshots were collected every 6 fs for post-simulation analysis. Chemical reactions were traced and analysed for the total simulation time of 11 ps.

We investigated system size effects using the computationally efficient density functional tight-binding[42] (DFTB) technique with self-consistent charges on a larger simulation cell based on a $2 \times 1 \times 2$ supercell. The concentration histories of the major species discussed here were investigated for possible size dependence. The concentration fluctuations in the larger simulations were less than those in the smaller simulations, but the concentration trends were very similar. This is consistent with our observations that PETN decomposition is unimolecular and that the majority of reactions are localized events. Smaller time steps were also investigated using DFTB. We found the concentration histories with a 0.5-fs time step to be similar to those determined with a 1.2 fs time step.

Post-simulation analysis. To analyse the MD snapshots, we defined chemical species on the basis of a set of bond distances (obtained from the radial distribution function) and a minimum-bond-lifetime criterion[20], which is used to distinguish between transient configurations and stable chemical species. Two atoms were not considered bonded unless they stayed continuously within the bond-distance criterion during the chosen minimum bond lifetime of 12 fs. Shorter or longer bond-lifetime criteria (6–30 fs) were also tested. Although the concentrations of species depend quantitatively on the specific choice of bond criteria, no effect was found on the qualitative conclusions reached in this work. Reaction events were then traced between snapshots, with rate constants determined by the traced elementary rate equation and concentrations of the species. To estimate Mulliken[43] charges, the mixed basis set CP2K code[44] was used with a cutoff of 400 Ry, a double-zeta basis set (DZVP)[45] and a PBE exchange-correlation function.

We used the Nerst–Einstein relation[35] to calculate the ionic conductivity

$$\sigma = \frac{1}{k_B T} \sum_i n_i q_i^2 D_i (1 - \Delta)$$

where n_i, q_i and D_i are the number density, charge and self-diffusion constant of species i, and Δ is a deviation parameter due to transient cross-correlations between the velocities of different ions[32]. As the atomic self-diffusion constants suggest that the mobility of the hydrogen population is much greater than that of the other species, we assumed that the slow-moving population in which hydrogen travels can

be described by a single self-diffusion constant D_{slow}, which we approximate by the average of the carbon, nitrogen and oxygen values. The ionic conductivity can then be written as

$$\sigma = \frac{n_H q_H^2}{k_B T}\left[D_H + D_{slow}\left(\frac{\langle q^2\rangle}{x_H q_H^2} - 1\right)\right](1-\Delta)$$

where $x_H = n_H/n_{total}$. As the dielectric constant in reacting PETN is close to that of a molten salt, we approximated its value of Δ using the averaged value of 0.26 for molten salts (approximate range of 0.08–0.43) published in a previous study[31]. That is, we have assumed that 26% of the mobile hydrogen atoms form transient dynamic complexes with the heavier background ions, which contribute to diffusive motion but not to electrical current. This assumption is based on our previous observation that the dielectric properties of the system are very similar to those of molten salts.

Received 24 December 2008; accepted 4 February 2009; published online 19 March 2009

References

1. Hubbard, W. B. Neptune's deep chemistry. *Science* **275,** 1279–1280 (1997).
2. Cavazzoni, C. *et al.* Superionic and metallic states of water and ammonia at giant planet conditions. *Science* **283,** 44–46 (1999).
3. Hemley, R. J. *et al.* Static compression of H_2O-ice to 128 GPa (1.28 Mbar). *Nature* **330,** 737–740 (1987).
4. Goncharov, A. F., Struzhkin, V. V., Somayazulu, M. S., Hemley, R. J. & Mao, H. K. Compression of ice to 210 gigapascals: Infrared evidence for a symmetric hydrogen-bonded phase. *Science* **273,** 218–220 (1996).
5. Goncharov, A.F. *et al.* Dynamic ionization of water under extreme conditions. *Phys. Rev. Lett.* **94,** 125508 (2005).
6. Goldman, N., Fried, L. E., Kuo, I. F. W. & Mundy, C. J. Bonding in the superionic phase of water. *Phys. Rev. Lett.* **94,** 217801 (2005).
7. Lin, J. F. *et al.* Melting behavior of H_2O at high pressures and temperatures. *Geophys. Res. Lett.* **32,** L11306 (2005).
8. Holmes, N. C., Nellis, W. J., Graham, W. B. & Walrafen, G. E. Spontaneous Raman scattering from shocked water. *Phys. Rev. Lett.* **55,** 2433–2436 (1985).
9. Schwegler, E., Galli, G., Gygi, F. & Hood, R. Q. Dissociation of water under pressure. *Phys. Rev. Lett.* **87,** 265501 (2001).
10. Ding, Z. Y., Frisch, M. A., Li, L. & Gloyna, E. F. Catalytic oxidation in supercritical water. *Ind. Eng. Chem. Res.* **35,** 3257–3279 (1996).
11. Farinacci, N. T. & Hammett, L. P. Polymolecular solvolytic reactions: Water catalysis in the alcoholysis of benzhydryl chloride. *J. Am. Chem. Soc.* **59,** 2542–2546 (1937).
12. Vohringer-Martinez, E. *et al.* Water catalysis of a radical-molecule gas-phase reaction. *Science* **315,** 497–501 (2007).
13. Smith, I. Single-molecule catalysis. *Science* **315,** 470–471 (2007).
14. Ree, F. H. A statistical mechanical theory of chemically reacting multiphase mixtures: Application to the detonation properties of PETN. *J. Chem. Phys.* **81,** 1251–1263 (1984).
15. Fried, L. E. & Howard, W. M. An accurate equation of state for the exponential-6 fluid applied to dense nitrogen. *J. Chem. Phys.* **109,** 7338–7348 (1998).
16. Ng, W. L., Field, J. E. & Hauser, H. M. Thermal, fracture, and laser-induced decomposition of pentaerythritol tetranitrate. *J. Appl. Phys.* **59,** 3945–3952 (1986).
17. Gruzdkov, Y. A. & Gupta, Y. M. Shock wave initiation of pentaerythritol tetranitrate crystals: Mechanism of anisotropic sensitivity. *J. Phys. Chem. A* **104,** 11169–11176 (2000).
18. Yoo, C. S. *et al.* Anisotropic shock sensitivity and detonation temperature of pentaerythritol tetranitrate single crystal. *J. Appl. Phys.* **88,** 70–75 (2000).
19. Tarver, C. M., Tran, T. D. & Whipple, R. E. Thermal decomposition of pentaerythritol tetranitrate. *Propell. Explos. Pyrot.* **28** 189–193 (2003).
20. Wu, C. J., Manaa, M. R. & Fried, L. E. Tight binding molecular dynamic simulation of PETN decomposition at an extreme condition. *Proc. Mater. Res. Soc.*, **987,** 139–144 (2007).
21. Manaa, M. R., Fried, L. E., Melius, C. F., Elstner, M. & Frauenheim, T. Decomposition of HMX at extreme conditions: A molecular dynamics simulation, *J. Phys. Chem. A* **106,** 9024–9029 (2002).
22. Strachan, A., van Duin, A. C. T., Chakraborty, D., Dasgupta, S. & Goddard, W. A. III Shock waves in high-energy materials: The initial chemical events in nitramine RDX. *Phys. Rev. Lett.* **91,** 098301 (2003).
23. Strachan, A., Kober, E. M., van Duin, A. C. T., Oxgaard, J. & Goddard, W. A. III Thermal decomposition of RDX from reactive molecular dynamics. *J. Chem. Phys.* **122,** 054502 (2005).
24. Nomura, K. *et al.* Dynamic transition in the structure of an energetic crystal during chemical reactions at shock front prior to detonation. *Phys. Rev. Lett.* **99,** 148303 (2007).
25. Reed, E. J., Manna, M. R., Fried, L. E., Glaesemann, K. R. & Joannopoulos, J. D. A transient semimetallic layer in detonating nitromethane. *Nature Phys.* **4,** 72–76 (2008).
26. Westbrook, C. K. & Dryer, F. L. Chemical kinetic modeling of hydrocarbon combustion. *Prog. Energy Combust.* **10,** 1–57 (1984).
27. Westbrook, C. K. Chemical kinetics of hydrocarbon ignition in practical combusion systems. *Proc. Combust. Inst.* **28,** 1563–1577 (2000).
28. Giguere, P. A. Great fallacy of the H^+ ion and the true nature of H_3O^+. *J. Chem. Educ.* **56,** 571–575 (1979).
29. Pauling, L. *The Nature of the Chemical Bond* 90 (Cornell Univ. Press, 1960).
30. Bastea, S. & Fried, L. E. Exp6-polar thermodynamics of dense supercritical water. *J. Chem. Phys.* **128,** 174502 (2008).
31. Hansen, J. P. & McDonald, I. R. Statistical mechanics of dense ionized matter. IV. Density and charge fluctuations in a simple molten salt. *Phys. Rev. A* **11,** 2111–2123 (1975).
32. Wilke, S. D., Chen, H. C. & Bosse, J. Dielectric and transport properties of a supercooled symmetrical molten salt. *Phys. Rev. E.* **60,** 3136–3149 (1999).
33. Clipper Controls. *Dielectric Constant Reference Guide* <http://clippercontrols.com/info/dielectric_constants.html> (2007).
34. Hayes, B. On electrical conductivity in detonation products. *Proc. 4th Int. Symp. Detonation, White Oak, Massachusetts* 595–601 (Office of Naval Research, Department of the Navy, October 1965).
35. Weinert, U. & Mason, E. A. Generalized Nernst–Einstein relations for nonlinear transport coefficients. *Phys. Rev. A* **21,** 681–690 (1980).
36. Booth, A. D. & Llewellyn, F. J. The crystal structure of pentaerythritol tetranitrate. *J. Chem. Soc.* 837–846 (1947).
37. Trotter, J. Bond lengths and angles in pentaerythritol tetranitrate. *Acta Crystallogr.* **16,** 698–699 (1963).
38. Yang, L. H., Hood, R. Q., Pask, J. E. & Klepeis, J. E. Large-scale quantum mechanical simulations of high-*Z* metals. *J. Computer-Aided Mater. Design* **14,** 337–347 (2007).
39. Perdew, J. P., Burke, K. & Ernzerhof, M. Generalized gradient approximation made simple. *Phys. Rev. Lett.* **77,** 3865–3868 (1996).
40. Troullier, N. & Martins, J. L. Efficient pesudopotentials for plane-wave calculations. *Phys. Rev. B* **43,** 1993–2006 (1991).
41. Brown, D. & Clarke, J. H. R. A comparison of constant energy, constant temperature and constant pressure ensembles in molecular-dynamics simulations of atomic liquids. *Mol. Phys.* **51,** 1243–1254 (1999).
42. Frauenheim, T. *et al.* A self-consistent charge density-functional based tight-binding method for predictive materials simulations in physics, chemistry and biology. *Phys. Status Solidi B* **217,** 41–62 (2000).
43. Mulliken, R. S. Electron population analysis on LCAO-MO molecular wave functions. *J. Chem. Phys.* **23,** 1833–1840 (1955).
44. CP2K Developers Group. *CP2K Code* <http://cpk2.berlios.de> (2000–2006).
45. Van de Vondele, J. *et al.* Quickstep: Fast and accurate density functional calculations using a mixed Gaussian and plane waves approach. *Comput. Phys. Commun.* **167,** 103 (2005).

Acknowledgements

This work was performed under the auspices of the US Department of Energy by Lawrence Livermore National Laboratory (LLNL) under Contract DE-AC52-07NA27344. The project 06-SI-005 was funded by the Laboratory Directed Research and Development Program at LLNL. The authors would like to express their sincere appreciation to E. Reed for useful discussion and to L. Krauss, K. Kline and J. McInnis for their contributions to the preparation of the manuscript and figures.

Author contributions

C.J.W. originated the central idea, performed and analysed the PETN MD simulations, and wrote the paper; L.E.F. developed the molecular analyser code and contributed to the writing of the paper; L.H.Y. carried out Quantum MD code development; N.G. contributed to Mulliken charge analysis; S.B. performed conductivity and dielectric constant calculations; all of the authors contributed to discussions and editing of the manuscript.

Additional information

Supplementary Information accompanies this paper at www.nature.com/naturechemistry. Reprints and permission information is available online at http://npg.nature.com/reprintsandpermissions/. Correspondence and requests for materials should be addressed to C.J.W.